Hopf bifurcation in the evolution of networks driven by spike-timing-dependent plasticity

Quansheng Ren, Kiran M. Kolwankar, Areejit Samal, and Jürgen Jost

Hopf bifurcation in the evolution of STDP-driven networks

Quansheng Ren[1,2],[*] Kiran M. Kolwankar[3,2],[†] Areejit Samal[4,2],[‡] and Jürgen Jost[2,5][§]

[1]*School of Electronics Engineering and Computer Science,*

Peking University, Beijing 100871, China

[2]*Max Planck Institute for Mathematics in the Sciences,*

Inselstrasse 22, D-04103 Leipzig, Germany

[3]*Department of Physics, Ramniranjan Jhunjhunwala College,*

Ghatkopar (W), Mumbai 400 086, India

[4]*Laboratoire de Physique Théorique et Modèles Statistiques,*

CNRS and Univ Paris-Sud, UMR 8626, F-91405 Orsay, France and

[5]*The Santa Fe Institute, 1399 Hyde Park Road,*

Santa Fe, New Mexico 87501, USA

Abstract

We study the interplay of topology and dynamics in a neural network connected with spike-timing-dependent plasticity (STDP) synapses. Stimulated with periodic spike trains, the STDP-driven network undergoes a synaptic pruning process and evolves to a residual network. We examine the variation of topological and dynamical properties of the residual network by varying two key parameters of STDP: Synaptic delay and the ratio between potentiation and depression. Our extensive numerical simulations of the Leaky Integrate-and-Fire model show that there exists two regions in the parameter space. The first corresponds to fixed point configurations, where the distribution of peak synaptic conductances and the firing rate of neurons remain constant over time. The second corresponds to oscillating configurations, where both topological and dynamical properties vary periodically which is a result of a fixed point becoming a limit cycle via a Hopf bifurcation. This leads to interesting questions regarding the implications of these rhythms in the topology and dynamics of the network for learning and cognitive processing.

[*] qsren@pku.edu.cn

[†] kiran.kolwankar@gmail.com

[‡] samal@mis.mpg.de

[§] jost@mis.mpg.de

I. INTRODUCTION

Adaptive networks arise in diverse areas ranging from neural learning [1, 2] to social dynamics [3, 4]. (For a review see Ref. [5].) Such networks combine topological evolution of the network with dynamics in the state of the nodes. In such networks, there are two types of evolution: (a) the edges between nodes get modified, pruned or rewired over time and (b) the state of the nodes can change over time. In adaptive networks, the two evolutions are explicitly coupled and can drive each other with complex feedback. Detailed investigation of the dynamics of this co-evolutionary process can lead to important insights on complex adaptive systems. Recent studies show the emergence of interesting physical phenomena due to this combined dynamics in adaptive networks. For example, a topological phase transition for some critical value of edge rewiring probability was observed for both social dynamics [6] and neural network models [7, 8]. Although, such studies have revealed some interesting phenomena in adaptive networks, there are many more interesting issues that still need to be addressed.

In neural networks, one of the learning paradigms for spiking neurons is spike-timing-dependent plasticity (STDP) [9]. STDP is an adaptive scheme that plays an important role in the interplay between the topology and dynamics of neural networks. STDP determines the evolution of synaptic weights based on pre- and post-synaptic activity, which in turn, changes the neuronal activity. Previous studies of STDP-driven networks have mainly investigated the influence of STDP rule on either the dynamics or the topology of neural networks. It has been shown that STDP could result in spike train learning [10] and enhancement or decoupling effect of synchronization [11, 12]. The topological evolution of STDP-driven networks is also well characterized. In Ref. [13], it was shown that the functional architecture of brain can self-organize into small-world and scale-free network via STDP mediated synaptic reorganization. Takahashi et al. [2] have studied the role of STDP in the development of feed-forward architecture in neural networks. Gilson et al. [14] have developed a framework to analyze systematically the behaviour of STDP in recurrent networks. It has also been suggested that the interplay between dynamics and topology might be essential for neural information processing [15].

Previous studies have established that STDP could drive a globally connected network to a steady-state condition where the firing rate of neurons and the distribution of peak synaptic conductances remain constant over time [9, 13, 15–18]. Specifically, in Ref. [17],

2

we have studied a network of neurons with STDP learning rule and properly chosen input signals. Starting from a globally connected network with random initial synaptic strengths, we found that majority of synapses weaken in the course of dynamics due to STDP rule leading to a sparse residual network. Moreover, such residual networks obtained by starting from different configurations of initial synaptic strengths were found to be different with some common characteristic properties. This observation indicates that the combined dynamics has several fixed points with each having its own basin of attraction in the high dimensional space of synaptic strengths. In our earlier contribution, we have established the robustness of the observed characteristic properties in the residual STDP-driven network for a narrow range of two key parameters in STDP learning rule: (a) the synaptic delay and (b) the ratio between potentiation and depression. We had also found there a striking similarity in the network motif distribution of the residual STDP-driven network in comparison to the real *C. elegans* neural network.

Our previous observations are expected to have important implications for neural information processing. Hence, in the present contribution, we have asked the following question: Are the fixed point steady states leading to the residual networks stable. In Fig. 1, we report results from a simulation of the Hodgkin-Huxley (HH) model that point to a bifurcation transition. From this figure, we can clearly see that there are two different long time behaviours for the number of synapses and the firing rate for different values of the parameters. Since simulations of HH model are more time consuming we have considered the Leaky Integrate-and-Fire (LIF) model to investigate this question in detail. This allows us to explore a wider range of parameter space. Here, through extensive numerical simulations of the LIF model, we report a bifurcation, a supercritical Hopf bifurcation, giving rise to a limit cycle. Hence, the parameter space can be divided into two distinct regions: one corresponding to fixed point configurations and the other to oscillating configurations where both topological and dynamical properties vary periodically. These new observations have interesting consequences for the network structure as a whole.

The rest of the paper is organized as follows: Section II describes the LIF model along with the spike-timing-dependent plasticity (STDP) rule. Section III presents results of our numerical simulations showing a Hopf bifurcation. Section IV presents network motif analysis of the resulting networks. The last section V concludes with discussion of the obtained results.
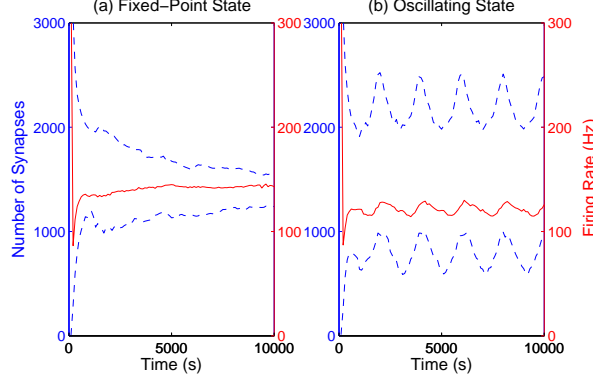
FIG. 1. (Color online) Evolution of the number of survived synapses (upper dashed line), the number of near-maximum synapses (lower dashed line), and the average firing rate of neurons (solid line) for two different evolutionary behaviours of the Hodgkin-Huxley (HH) model: (a) fixed point state, (b) oscillating state. The chosen parameters are depicted by squares in Fig. 6(a).

II. NEURON MODELS AND STDP LEARNING RULE

The Network were modeled using the NEST Simulation Tool [19]. We have used the Leaky Integrate-and-Fire (LIF) model to simulate the behaviour of neurons. The membrane potential of the conductance based LIF neuron is described by:

$$C_m \frac{dV_j}{dt} = g_L(V_r - V_j) + g_j(t)(E_{ex} - V_j) , \tag{1}$$

where $C_m = 200$pF is the membrane capacitance, V_j is the membrane potential of the jth neuron, $g_L = 10$nS is the leak conductance which is equivalent to $R_m = 100$MΩ with R_m as the membrane resistance, $V_r = -70$mV is the resting potential (leak reversal potential), and $E_{ex} = 0$mV is the excitatory reversal potential. When the membrane potential reaches the threshold value ($V_{th} = -54$mV), the neuron emits an membrane potential, and the depolarization is reset to reset potential ($V_r = -60$mV) after a refractory period ($\tau_{ref} = 1$ms) during which the potential is insensitive to stimulation. The parameters used here are same as in Ref. [9].

The Traub modified conductance based Hodgkin-Huxley model neuron is used to obtain Fig. 1. It is described by the following equation:

$$C_m \frac{dV_j}{dt} = g_L(E_L - V_j) + g_{Na}m^3h(E_{Na} - V_j) + g_K n^4(E_K - V_j) + g_j(t)(E_{ex} - V_j), \tag{2}$$

where $C_m = 100$pF. $E_{ex} = 0$mV is the excitatory reversal potential. The maximal conductances and reversal potentials of the sodium and potassium ion channels and the leak

4

channel used in the model are $g_{Na} = 1.0\text{mS/mm}^2$, $g_K = 2.0\text{mS/mm}^2$, $g_L = 0.001\text{mS/mm}^2$, $E_{Na} = 48\text{mV}$, $E_K = -82\text{mV}$, and $E_L = -67\text{mV}$ respectively. The gating variables $X = m, h, n$ satisfy the following equation:

$$\frac{dX}{dt} = \alpha_X(V_j)(1 - X) - \beta_X(V_j)X, \tag{3}$$

where α_X and β_X are given by

$$\alpha_m = \frac{0.32(V + 54)}{1 - \exp(-0.25(V + 54))} \beta_m = \frac{0.28(V + 27)}{\exp(0.2(V + 27)) - 1}$$

$$\alpha_h = 0.128 \exp(-(V + 50)/18) \beta_h = \frac{4}{1 + \exp(-0.2(V + 27))}$$

$$\alpha_n = \frac{0.032(V + 52)}{1 - \exp(-0.2(V + 52))} \beta_n = 0.5 \exp(-(V + 57)/40).$$

These parameters are taken from [20].

The synaptic conductance $g_j(t)$ of the jth neuron at time t in Eq. (1) is given by:

$$g_j(t) = g_m \sum_{i=1}^{N} w_{ij}(t) \sum_k f(t - t_i^k), \tag{4}$$

where N is the number of neurons, g_m is the maximum value of synaptic conductance, w_{ij} is the weight of the synaptic connection from the ith neuron to the jth neuron, t_i^k is the timing of the kth spike of the ith neuron. In Eq. (4), we have used an α-function [21] $f(t)$ with latency (or transmission delay) τ_d and synaptic time constant $\tau_{ex} = 2\text{ms}$:

$$f(t) = \begin{cases} \frac{t - \tau_d}{\tau_{ex}^2} \exp(-\frac{t - \tau_d}{\tau_{ex}}) & \text{if } t > \tau_d \\ 0 & \text{otherwise.} \end{cases} \tag{5}$$

In this study, the weight of the synaptic connection w_{ij} gets modified via STDP learning rule. The STDP rule is a form of experimentally observed long-term synaptic plasticity where synaptic strengths get modified by repeated pairings of pre- and post-synaptic membrane potentials with the sign and the degree of the modification dependent on the relative timing of the firing of neurons. The amount of modification is determined based on the temporal difference Δt between the occurrence of the post-synaptic membrane potential and the arrival of the pre-synaptic membrane potential,

$$\Delta t = t_j - (t_i + \tau_d), \tag{6}$$

where t_j is the spike time of the postsynaptic neuron j, t_i is the spike time of the presynaptic neuron i, and τ_d is the delay time of the spike transmission from neuron i to neuron j.

The weight modification Δw_{ij} is described by the following equation, which is applied at postsynaptic spikes:

$$\Delta w_{ij}(\Delta t) = \begin{cases} \lambda \exp(-|\Delta t|/\tau_+) & \text{if } \Delta t \geq \tau_d \\ -\lambda\alpha \exp(-|\Delta t|/\tau_-) & \text{if } \Delta t < \tau_d, \end{cases} \quad (7)$$

where $\lambda = 0.0001$ is the learning rate. Here, we have chosen a small learning rate to simulate the effect of STDP on the long term development of neural system. The synaptic strengths w_{ij} is constrained within the range $[0, 1]$ which ensures that the peak synaptic conductance $g_m w_{ij}$ is always positive and cannot exceed the maximum value $g_m = 0.3nS$. The time constants τ_+ and τ_- controls the width of the time window, and α introduces a possible asymmetry between the scale of potentiation and depression. As argued in Ref. [9], in order to obtain stable competitive synaptic modification, i.e., uncorrelated pre- and post-synaptic spikes producing an overall weakening of synapses, the integral of Δw_{ij} should be negative. Here, we have used an asymmetric time window of $\tau_+ = 16.8$ms and $\tau_- = 33.7$ms for STDP rule which provides a reasonable approximation of the synaptic modification observed in experiments [22]. The choice of $\alpha > 0.5$ along with an asymmetric time window results in a ratio of $\alpha\tau_-/\tau_+ > 1.0$ ensuring that the integral of Δw_{ij} is negative.

III. HOPF BIFURCATION IN THE COEVOLUTION OF TOPOLOGY AND DYNAMICS

We now investigate how the topology and dynamics evolve together over time in STDP-driven networks. In our simulations, we start from a globally connected network of 100 neurons with membrane potentials of neurons initialized to a value drawn at random from a clipped normal distribution, with mean potential -57.0 mV, variance 3.0 mV, and maximum -54.0 mV (threshold potential). The synapses of the network are governed by STDP learning rule. The peak synaptic conductances are initialized to a clipped normal distribution, with mean 0.15 nS, variance 0.15 nS and minimum 0.0 nS. We use a small learning rate ($\lambda = 0.0001$) and run the simulations for time $t > 10^7$ms in order to mimic long term development of neural systems. The neurons are stimulated repeatedly by different patterns that have a period of $T_p = 150ms$ and are truncated from independent Poisson spike trains with the same average rate $f_{ps} = 50$Hz, which is analogous to the stimulus scheme in [23]. The average firing rate corresponds to a 20ms spike interval which is consistent with the width of
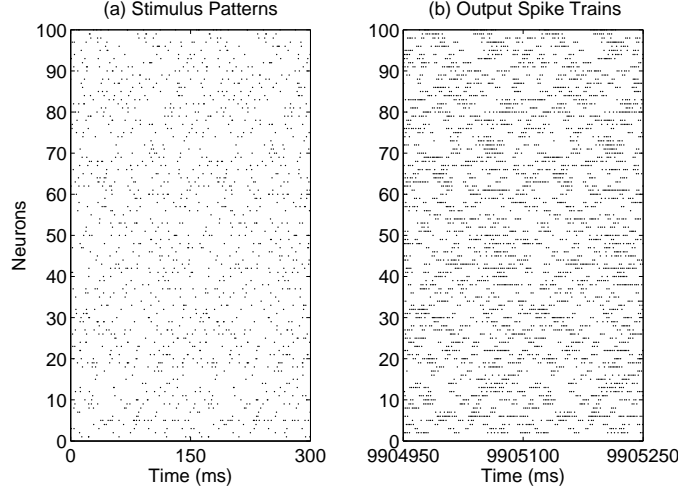
6

FIG. 2. Spatio-temporal spike patterns: (a) two successive periods of the input stimulus patterns of 100 neurons, (b) an example of the output spike trains in the final stage of the evolution of STDP-driven network, where $\alpha = 0.71$ and $\tau_d = 2.0$ms.

STDP time window. The stimulus patterns are visualized in Fig. 2(a), where two successive periods of stimulus patterns are shown.

Several authors have shown that after a period of relaxation by STDP, a fixed point condition can be achieved, where the firing rate of the post-synaptic neuron and the distribution of peak synaptic conductances become constant [9, 13, 16, 17]. During the learning process due to the asymmetry between the scale of potentiation and depression, most of the synapses get weakened to nearly zero while others get strengthened to achieve the maximum conductance. The distribution of peak synaptic conductances approaches a bimodal distribution in resulting networks. However, the previously published results were obtained for a limited range in parameter space. Here, we have investigated this issue in a wider range of parameter space.

We have examined the variation of topological and dynamical properties of STDP-driven networks by varying two key parameters of STDP rule: (a) synaptic delay τ_d within a range of 1-15 ms and (b) the ratio between potentiation and depression α within a range of 0.50-0.74. In each simulation, we start from a globally coupled network along with specific values for τ_d and α. The STDP-driven network then undergoes a synaptic pruning process and evolves to a residual network. In this work, we find that the residual network is either in a fixed point state or an oscillating state depending on the value of τ_d and α.

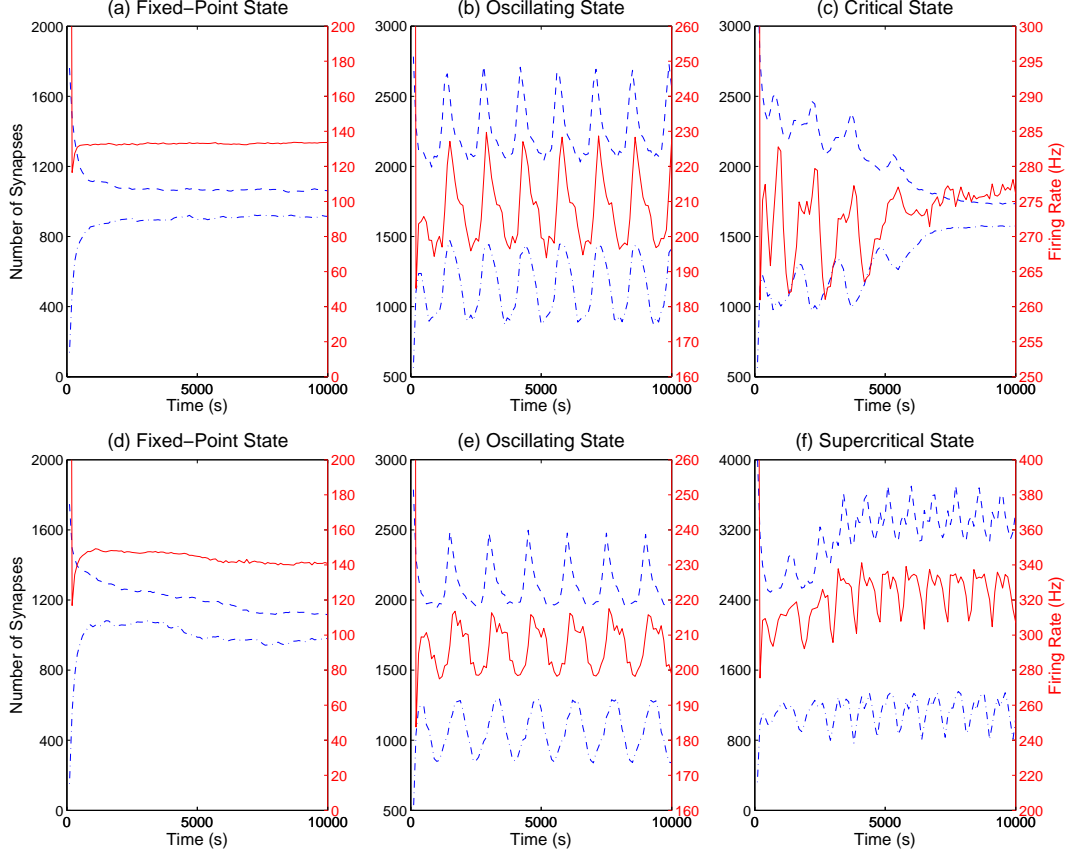To study the topological and dynamical characteristics of the coevolution process, two

7

FIG. 3. (Color online) Evolution of the number of survived synapses (dashed line), the number of near-maximum synapses (dash-dot line), and the average firing rate of neurons (solid line) for the examples of the four different evolutionary behaviours: (a) fixed point state ($\alpha = 0.71, \tau_d = 2.0$ms), (b) oscillating state ($\alpha = 0.6, \tau_d = 6.0$ms), (c) critical state ($\alpha = 0.54, \tau_d = 8.0$ms), and (f) supercritical state ($\alpha = 0.52, \tau_d = 5.0$ms). The robustness of the fixed-point state and the oscillating state against heterogeneous delays is shown in (d) and (e), where α is 0.71 and 0.6 respectively and the synaptic delays τ_d are randomly selected with a uniform distribution from the interval [0.1 ms, 15.0 ms] in both cases.

properties of the residual network are monitored. The first property is the average firing rate of neurons which gives an overview of network dynamics. The second property is the number of synapses that have strength greater than a certain threshold. To inspect the topological characteristics of the residual network, we filter the adjacency matrix using two types of threshold. In the first case, we use a small threshold of $g_s = 0.01$nS. If the weight of a synapse is greater than the threshold value then it is considered a survived synapse, otherwise considered a pruned synapse. From the filtered adjacency matrix, the number of
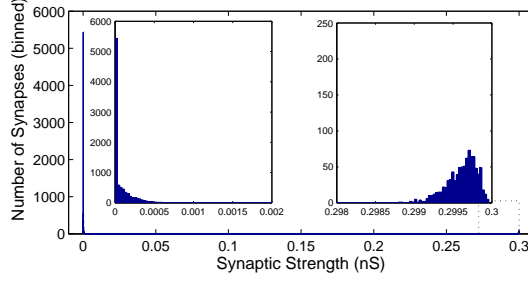
FIG. 4. (Color online) The bimodal distribution of peak synaptic conductances in the residual network for fixed point state, where $\alpha = 0.71, \tau_d = 2.0$ms.
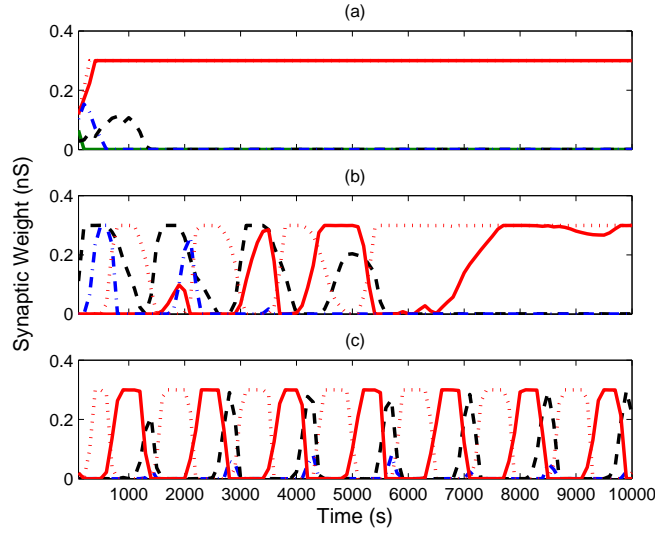

FIG. 5. (Color online) Evolution of synaptic conductances for the three different evolutionary behaviours: (a) fixed point state ($\alpha = 0.71, \tau_d = 2.0$ms), where the synapses g_{26-36}, g_{30-40}, g_{54-64}, g_{61-71} and g_{89-99} are shown; (b) oscillating state ($\alpha = 0.6, \tau_d = 6.0$ms), where the synapses g_{2-12}, g_{5-15}, g_{6-16} and g_{20-30} are shown; and (c) critical state ($\alpha = 0.54, \tau_d = 8.0$ms), where the synapses g_{6-16}, g_{12-22}, g_{20-30} and g_{80-90} are shown.

survived synapses is estimated. In the second case, we use a large threshold of $g_l = 0.29$nS which gives us the number of synapses approaching the maximum value ($g_m = 0.3nS$) or number of near-maximum synapses from the filtered adjacency matrix. Fig. 3 show three different behaviours observed in our simulations for the properties monitored for different values of parameters τ_d and α.

Fig. 3(a) shows the case of the fixed point state where $\alpha = 0.71$ and $\tau_d = 2.0$ms. This case has been reported in earlier studies [9, 13, 15–17]. It can be seen that the number of survived synapses ($> g_s = 0.01$nS) decreases rapidly until 10^6ms after which it remains almost
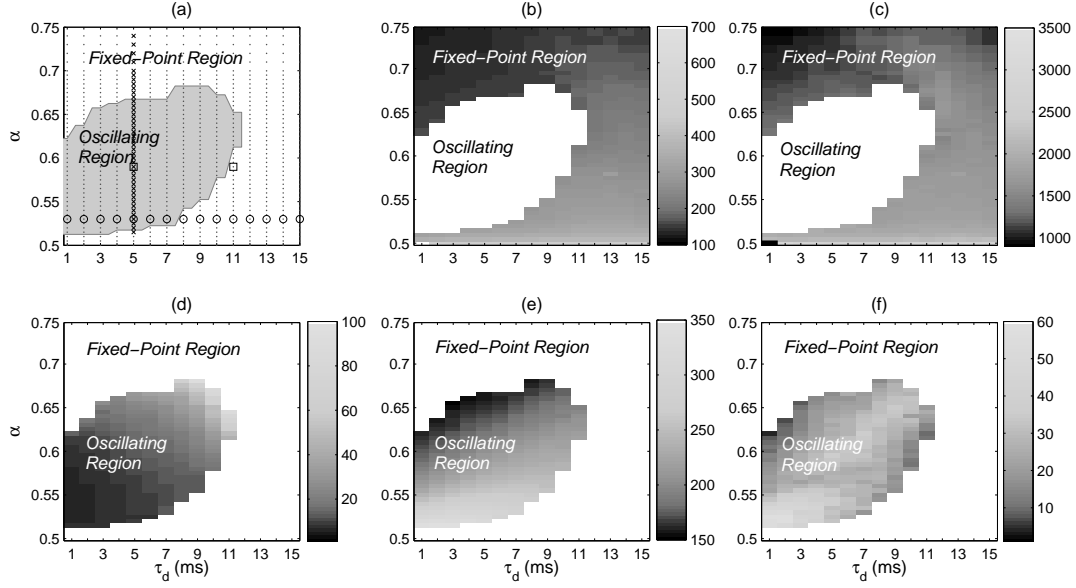
FIG. 6. Two parameter phase diagram showing the dependence of STDP-driven networks on the value of two key parameters: α which is the ratio between potentiation and depression, and τ_d which is the synaptic delay. (a) The evolutionary behaviour can be classified into two categories: fixed point state (white region) and oscillating state (grey region). Every dot symbol corresponds to a simulation case. The vertical line (cross symbols) and the horizontal line (circle symbols) show configurations corresponding to the simulations in Fig. 8(d) and (c) respectively, where either $\tau_d(=5)$ms or $\alpha(=0.53)$ is fixed while the other parameter traverses a vast range. The two square symbols depict parameters corresponding to the simulations of HH model shown in Fig. 1. (b) The average firing rate (in Hz), and (c) the number of survived synapses for different configurations in the fixed point region. (d) The oscillation period (in 100s), (e) the mean, and (f) the amplitude of the average firing rate fluctuations (in Hz) corresponding to different configurations in oscillating region.

constant. The fraction of the synapses survived at the end is 10.7% of the total, indicating that most of the synapses in fact did not survive. However, the number of near-maximum synapses ($> g_l = 0.29$nS) increases rapidly until 10^6ms after which it remains almost constant (about 9.2% of the total). The difference between the number of survived synapses and number of near-maximum synapses is approximately 150 implying that synapses whose strength lies between $g_s = 0.01$nS and $g_l = 0.29$nS account for a small fraction of survived synapses. Fig. 4 shows the bimodal distribution of synaptic strengths in residual networks.

10

The evolution of average firing rate of neurons shows a trend similar to number of survived synapses and number of near-maximum synapses (cf. Fig. 5(a)).

In our simulations, apart from the fixed point case, an oscillating state of the residual network is also discovered. An example of oscillating state is shown in Fig. 3(b) where $\alpha = 0.6$ and $\tau_d = 6.0$ms. We find that the number of survived synapses (or near-maximum synapses) decrease (increase) to a certain level and fluctuate in a certain range, about 20.5%-27.5% (9.0%-14.5%) of the total, with the period of 1450s. Due to the interplay between dynamics and structure of the network, the average firing rate also oscillates with the same period. After the transient period ($t > 10^6$ms), we have determined the mean and amplitude of this oscillation which are equal to 211.7 and 33.9, respectively. Fig. 5(b) shows that typical synaptic conductances also oscillate over whole range of allowed values with the same period.

The robustness of the fixed-point state and the oscillating state against heterogeneous delays is shown in Fig. 3(d) and (e), where α is 0.71 and 0.6 respectively and the synaptic delays τ_d are randomly selected with a uniform distribution from the interval [0.1 ms, 15.0 ms] in both cases. For the case of $\alpha = 0.71$, the synaptic delays between [0.1 ms, 15.0 ms] all lie in the fixed-point region. For the case of $\alpha = 0.6$, the boundary between the oscillating region and the fixed-point region is between 10.0 ms and 11.0 ms. Thus the fixed-point configurations within [11.0 ms, 15.0 ms] contribute to the evolution of the network also, reflected in smaller amplitudes of the oscillations of Fig. 3(e) compared with that of Fig. 3(b).

An interesting question is what happens when the parameters cross the critical value at the boundary between the fixed-point region and the oscillating region in parameter space. An example is showed in Fig. 3(c) where $\alpha = 0.54$ and $\tau_d = 8.0$ms. One can see that the number of survived synapses (or near-maximum synapses) show damped oscillations asymptotically approaching and finally achieving the level of the fixed point state. Similarly, the average firing rate also evolves toward a fixed point state with damped oscillations. The synaptic conductances also show similar behaviour (cf. Fig. 5(c)). These observations clearly indicate the existence of a Hopf bifurcation from fixed points in the high dimensional space of synaptic strengths to a limit cycle. To determine the character of the Hopf bifurcation, we further report an example of a supercritical state in Fig. 3(f) where $\alpha = 0.52$ and $\tau_d = 5.0$ms. Here, a small-amplitude limit cycle appears immediately after the fixed point goes unstable indicating a supercritical Hopf bifurcation.

We have done extensive numerical simulations to examine the coevolutionary behaviour

of the residual network in a wide range of the parameter space for α and τ_d. Based on the three different observed behaviours mentioned above, the whole parameter space could be separated into two regions as shown in Fig. 6(a). The first corresponds to fixed point configurations where the distribution of peak synaptic conductances and the firing rate remains constant over time (cf. Fig. 3(a)). The second corresponds to oscillating configurations where topological and dynamical properties both vary periodically in time (cf. Fig. 3(b)). The results of the average firing rate and the number of survived synapses corresponding to different configurations in the fixed point region are shown in Fig. 6(b) and Fig. 6(c). As expected, the number of survived synapses and the firing rate decrease as the ratio between potentiation and depression α is increased. The results for the mean and amplitude of the average firing rate fluctuation corresponding to different configurations in the oscillating region are shown in Fig. 6(e) and Fig. 6(f). The mean value decreases monotonically with increasing α similar to the case of the fixed point configuration. However, the variation of the amplitude does not exhibit monotonically changing behaviour. On the other hand, Fig. 6(d) shows that the period of the oscillation of the firing rate increases monotonically with both α and τ_d. These different observed characteristics imply that the interplay between the potentiation and depression along with time delay could bring about complex behaviours during the coevolution of topology and dynamics.

Finally, there exist some variation with input too. As addressed in our previous paper [17], while increasing the length of repeated spike sequence or mixing with non-periodic stochastic spikes, the stochastic aspects of the spike trains dominate, and the number of surviving links become smaller, but the common characteristic properties we found do not change. In principle, the existence of a bifurcation transition reported in Fig. 1 also does not change for these cases. However, the oscillating region in parameter space may shrink or widen depending on the input. Here, we have adopted a reasonable type of input with a chosen period so as to be able to focus our attention on extensive numerical simulations of other parameter values. The important point here is that given the input, one observes an oscillating state for some parameters and a fixed point state for others.

IV.   NETWORK MOTIF ANALYSIS

We next perform network motif analysis [25, 26] to compare the structural characteristics of resulting networks for two different evolutionary behaviours. Network motifs are patterns
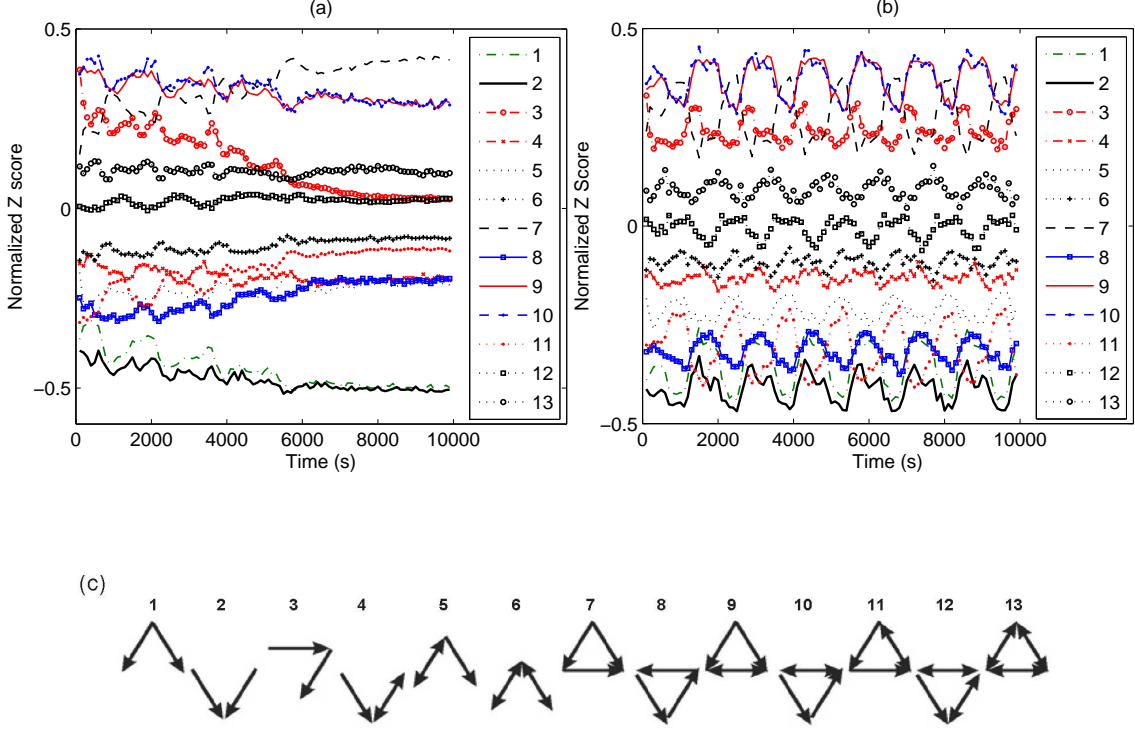
FIG. 7. (Color online) Evolution of Normalized Z-score for: (a) critical state ($\alpha = 0.54, \tau_d = 8.0$ms) and (b) oscillating state ($\alpha = 0.6, \tau_d = 6.0$ms). (c) The structure of the three node subgraph corresponding to each triad ID.

of interconnections (or sub-graphs) that recur in the real network much more often than expected at random. Network motif profile has been used to characterize diverse networks. Different sub-graphs have been shown to carry out different functions and the abundance of certain sub-graphs can determine the overall character of a network. In order to determine the over-representation or under-representation of sub-graphs in a real network, one needs to generate randomized versions of the real network and count the number of sub-graphs therein. We use the software Mfinder developed by Alon and co-workers [25, 26] for network motif analysis. We first obtain the frequency of different three-node sub-graphs in a given network and then compare it with the average frequency in an ensemble of 1000 random networks. Randomization is performed by rewiring connections such that the number of incoming edges, outgoing edges and mutual edges for each node is preserved.

The abundance of each sub-graph i is quantified by the Z-score,

$$z_i = \frac{N_i^{rl} - \langle N_i^{rd} \rangle}{\text{std}(N_i^{rd})}, \tag{8}$$

where N_i^{rl} is the abundance of sub-graph i in the real network, $\langle N_i^{rd} \rangle$ and $\text{std}(N_i^{rd})$ are the

13

mean and standard deviation of the abundance of sub-graph i in the ensemble of random networks. If $z_i > 0$ ($z_i < 0$) then the sub-graph i is over-represented (under-represented) and is designated as a motif (anti-motif) [25]. The significance profile (SP) of different sub-graphs in a network is the vector of Z-scores normalized to length 1:

$$S_i = \frac{z_i}{\sqrt{\sum_i^{13} z_i^2}}. \tag{9}$$

SP gives the relative significance of sub-graphs in a network and can be used to compare networks of different sizes and degree sequences [26]. We have studied the effect of the oscillating synaptic strengths on the motif SP and the results are contained in Fig. 7 and Fig. 8. Fig. 7 depicts the evolution of the normalized Z-score for different sub-graphs. We observe both oscillations and critical damping of Z-scores when the parameters lie in the relevant regions. We have determined the SPs of residual networks obtained for different parameter configurations. As the motif SPs oscillate in time for the configurations in the oscillating region, we have taken the network structure at a fixed time step, the end of the evolution, for all the cases. Fig. 8(b) shows the motif distribution averaged over an ensemble of independently evolved networks with different values of α and τ_d in the fixed-point region and in the oscillating region. Randomly generated membrane potentials and initial weights of STDP synapses are also used for different configurations, as has been explained in section II. For comparison, we depict the SP of *C. elegans* is depicted in Fig. 8(a). In contrast to vast diversity observed in the number of survived synapses and the average firing rate of different configurations (cf. Fig. 6(c) and Fig. 6(b)), the standard deviation is within a very small range. The robustness of SP is evident from this small standard deviation.

We have also studied the motif SP in different simulations where one of the two key parameters is kept fixed while the other is varied over a range. First, we fix α to 0.53, and then vary time delay τ_d in two regions. The first region contains values from 1ms to 7ms that lie within the oscillating region, and the second region has values from 8ms to 15ms that lie within the fixed-point region. As seen from the Fig. 8(c) if parameters occur within the oscillating region, then motif distributions corresponding to different τ_d are scattered in a certain range, though the form of SP characteristics is qualitatively preserved. However, the variation in the motif distributions is compact if the parameters lie in the fixed point region. Similar results are obtained in the case where the time delay is kept fixed at 5ms and the parameter α is varied in two different regions (cf. Fig. 8(d)).

14

V. CONCLUSIONS

We have studied the coevolution of structure and dynamics in a neural network where synaptic connections get modified by STDP learning rule. When stimulated by periodic spike trains, the STDP-driven network undergoes a synaptic pruning process and evolves to a residual network. In the present contribution, we focus on the influence of parameter variation to provide a more detailed insight compared to earlier studies. We have examined the variation in the observed topological and dynamical properties of the residual network as a consequence of varying two key parameters of STDP learning rule: (a) synaptic delay and (b) the ratio between potentiation and depression. Our extensive numerical simulations of the LIF model show that there exists two regions in the parameter space. The first corresponds to fixed point configurations where the distribution of peak synaptic conductances and the firing rate remains constant over time after the transient period. The second corresponds to oscillating configurations where structure and dynamical properties coevolve periodically due to their coupling via STDP. When the parameters cross the critical values at the boundary between the two regions, structure and dynamical properties coevolve with damped oscillation and asymptotically approach the fixed point state, which coincides with a Hopf bifurcation. Detailed studies of these phenomena show that the interplay between potentiation and depression of STDP along with time delay can lead to emergence of complex behaviors in the coevolution of structure and dynamics of residual network. Network motif analysis was also used to characterize the two different evolutionary behaviors of the residual network. We find that if parameters occur in the fixed point region then there is not much variation in the motif distribution. However, if parameters occur in the oscillating region, the motif distributions corresponding to different parameter values are scattered although the form of SP characteristics is qualitatively preserved.

Our study has led to some interesting questions. Various kinds of rhythms in brain and their role in the cognitive processing is well known and is an ongoing topic of active research [27]. However, the frequency of oscillations suggested by our simulations are much smaller than the rhythms studied hitherto. This is expected since the emergence of oscillatory behaviour in our numerical simulations is a consequence of the much slower learning dynamics. There is indeed a need to verify this prediction by carefully analyzing much longer signals for the existence of still slower oscillations. Further, there is a question of the implication of these rhythms in the structure and dynamics to memory and learning.

Are these rhythms desirable or otherwise? Would the brain be utilizing these oscillations for better cognitive processing? Future research would shed some light on these intriguing questions.

ACKNOWLEDGMENTS

[1] J.-M. P. Franosch, M. Lingenheil, and J. L. van Hemmen, Phys. Rev. Lett. **95**, 078106 (2005).

[2] Y. K. Takahashi, H. Kori, and N. Masuda, Phys. Rev. E **79**, 051904 (2009).

[3] C. Nardini, B. Kozma, and A. Barrat, Phys. Rev. Lett. **100**, 158701 (2008).

[4] G. Demirel, R. Prizak, P. Reddy, and T. Gross, Eur. Phys. J. B **84**, 541 (2011).

[5] T. Gross and B. Blasius, J. R. Soc. Interface **5**, 259 (2008).

[6] C. Castellano, S. Fortunato, and V. Loreto, Rev. Mod. Phys. **81**, 591 (2009).

[7] S. Bornholdt and T. Rohlf, Phys. Rev. E **67**, 066118 (2003).

[8] S. Bornholdt and T. Rohlf, Phys. Rev. Lett. **84**, 6114 (2000).

[9] S. Song, K. D. Miller, and L. F. Abbott, Nature Neuroscience **3**, 919 (2000).

[10] T. Masquelier, R. Guyonneau, and S. J. Thorpe, PLoS One **1**, e1377 (2008).

[11] V. P. Zhigulin, M. I. Rabinovich, R. Huerta, and H. D. I. Abarbanel, Phys. Rev. E **67**, 021901 (2003).

[12] E. V. Lubenov and A. G. Siapas, Neuron **58**, 118 (2008).

[13] C.-W. Shin and S. Kim, Phys. Rev. E **74**, 045101 (2006).

[14] M. Gilson, A. Burkitt, and J. L. van Hemmen, Front. Comput. Neurosci. **4**, 23 (2010).

[15] C. Meisel and T. Gross, Phys. Rev. E **80**, 061917 (2009).

[16] J. Jost and K. M. Kolwankar, Physica A **388**, 1959 (2009).

[17] Q. Ren, K. M. Kolwankar, A. Samal, and J. Jost, Physica A **389**, 3900 (2010).

[18] K. M. Kolwankar, Q. Ren, A. Samal, and J. Jost, Pramana - J. of Phys. **77**, 817 (2011).

[19] M.-O. Gewaltig and M. Diesmann, Scholarpedia **2**, 1430 (2007).

[20] R. D. Traub and R. Miles, *Neuronal Networks of the Hippocampus* (Cambridge University Press, Cambridge UK., 1991).

[21] N. Brunel and V. Hakim, Neural Computation **11**, 1621 (1999).

[22] G. qiang Bi and M. ming Poo, Annu. Rev. Neurosci. **24**, 139 (2001).

[23] T. Masquelier, R. Guyonneau, and S. J. Thorpe, PLoS ONE **1**, e1377 (2008).

[24] L. R. Varshney, B. L. Chen, E. Paniagua, D. H. Hall, and D. B. Chklovskii, PLoS Comput. Biol. **7**, e1001066 (2011).

[25] R. Milo, S. Shen-Orr, S. ltzkovitz, N. Kashtan, D. Chklovskii, and U. Alon, Science **298**, 824 (2002).

[26] R. Milo, S. Itzkovitz, N. Kashtan, R. Levitt, S. Shen-Orr, I. Ayzenshtat, M. Sheffer, and U. Alon, Science **303**, 1538 (2004).

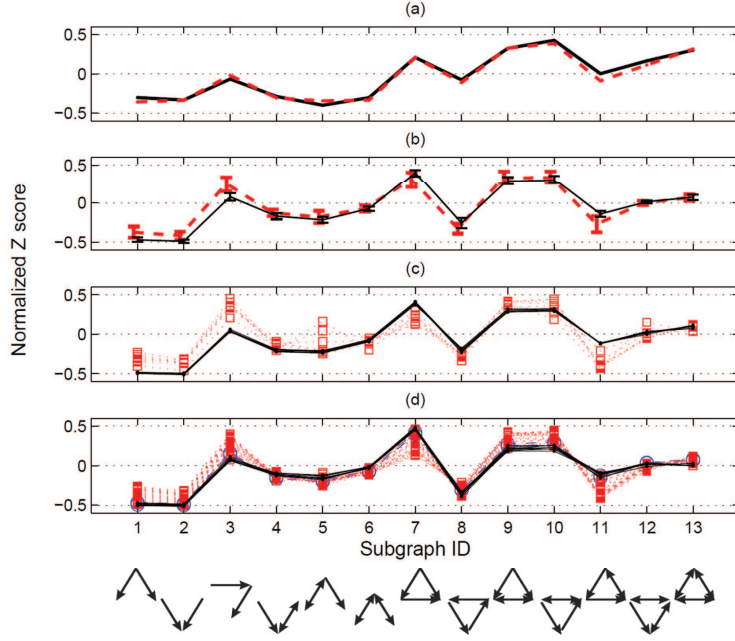[27] G. Buzsaki and A. Draguhn, Science **304**, 1926 (2004).

FIG. 8. (Color online) The triad significance profile (SP) of different networks. The normalized significance level (Z-score) for each of the 13 triads is shown, and the lines connecting the Z-score values serve only as visualization aid. The different networks are as follows: (a) The whole neuronal network (the dark solid line) and the inter neurons network (the red dashed line) in the *C. elegans* neural system. The latest wiring diagram of *C. elegans* neural system from Ref. [24] is used here. (b) Two ensembles of independently evolved STDP-driven networks with different parameter configurations (the charcoal grey points in Fig. 4(a)) of α and τ_d in fixed-point region (the dark solid line) and oscillating region (the red dashed line) respectively. The average and standard deviation of SP is calculated for each ensemble. (c) The SPs of the STDP-driven networks with fixed $\alpha = 0.53$ along with $\tau_d = 1 - 7$ms (the red dotted lines with square markers, oscillating-state configurations (OS)) or $\tau = 8 - 15$ms (the dark solid lines with point markers, fixed-point state configurations (FS)). (d) The SPs of the STDP-driven networks with fixed $\tau_d = 5$ms along with $\alpha = 0.51 - 0.515$ (the blue dashed line with circle marker, FS), $\alpha = 0.52 - 0.664$ (the red dotted lines with square markers, OS) or $\alpha = 0.67 - 0.74$ (the dark solid lines with point markers, FS). As the motif SPs oscillate in time for the configurations in the oscillating region, we have taken the network structure at a fixed time step, the end of the evolution, for all the cases.